Hindawi
International Journal of Photoenergy
Volume 2020, Article ID 1627498, 11 pages
https://doi.org/10.1155/2020/1627498

Research Article

Methylene Blue Photodegradation under Visible Irradiation on Ag-Doped ZnO Thin Films

William Vallejo, Alvaro Cantillo, and Carlos Díaz-Uribe

Grupo de Fotoquímica y Fotobiología, Facultad de Ciencias Básicas, Universidad del Atlántico, 081007 Puerto Colombia, Colombia

Correspondence should be addressed to William Vallejo; williamvallejo@mail.uniatlantico.edu.co

Received 4 September 2019; Revised 17 November 2019; Accepted 2 December 2019; Published 2 January 2020

Academic Editor: Zaiyong Jiang

This study synthesized and characterized Ag-doped ZnO thin films. Doped ZnO powders were synthesized using the sol-gel method, and thin films were fabricated using the doctor blade technique. The Ag content was determined by optical emission spectrometers with inductively coupled plasma (ICP plasma). Additionally, X-ray diffraction, Raman spectroscopy, Atomic Force Microscopy (AFM), diffuse reflectance, and X-ray photoelectron spectroscopy (XPS) measurements were used for physicochemical characterization. Finally, the photocatalytic degradation of methylene blue (MB) was studied under visible irradiation in aqueous solution. The Langmuir-Hinshelwood model was used to determine the reaction rate constant of the photocatalytic degradation. The physicochemical characterization showed that the samples were polycrystalline, and the diffraction signals corresponded to the ZnO wurtzite crystalline phase. Raman spectroscopy verified the ZnO doping process. The AFM analysis showed that roughness and grain size were reduced after the doping process. Furthermore, the optical results indicated that the presence of Ag improved the ZnO optical properties in the visible range, and the Ag-doped ZnO thin films had the lowest band gap value (2.95 eV). Finally, the photocatalytic degradation results indicated that the doping process enhanced the photocatalytic activity under visible irradiation, and the Ag-doped ZnO thin films had the highest MB photodegradation value (45.1%), as compared to that of the ZnO thin films (2.7%).

1. Introduction

The high concentration of organic dyes in wastewater has been a problem; synthetic dyes are recalcitrant compounds and are not completely degraded by conventional water treatments [1, 2]. Currently, the search for efficient, cheap, and green treatment processes for wastewater is a challenge around the world. In this context, the field of heterogeneous photocatalysis is aimed at synthesizing materials for the achievement of solar photodegradation processes (solar energy as a primary energy source) [3, 4]. Zinc oxide (ZnO) is a semiconductor frequently used in heterogeneous photocatalysis due to its particular properties (e.g., photochromic resistance, low toxicity, physical and chemical stability, high electron mobility, and suitable quantum yield) [5, 6]. Despite the fact that ZnO has been recognized as a promising photocatalyst, it has a high band gap value (~3.3 eV)—only 4% of the solar spectrum is effective to activate it. Therefore, improving the photoresponse of ZnO to longer wavelengths of the electromagnetic spectrum is the goal to be achieved for photocatalytic applications under solar irradiation [7]. Different strategies have been reported to extend photoresponse of semiconductors into the visible light region: (a) sensitization with natural and synthetic dyes [8–11], (b) coupled semiconductors [12–14], (c) surface plasmon resonance [15–18], and (d) doping ZnO structure with metals and nonmetals [19–21]. Among these, the doping process can modify the band gap of ZnO, generating electronic state intragap inside of the semiconductor thus ensuring the photoactivity redshift; on that topic, different authors have reported that ZnO changed photoresponse after the doping process [22].

The sol-gel method is a suitable technique for doping ZnO with different metals, as it is known that morphological, structural, optical, and photocatalytic properties rely on the synthesis conditions and the manufacturing method [23–25]. Different transition metals (e.g., Co^{2+}, Ag^{+}, Cu^{2+}, and Mn^{2+}) have been used to enhance photophysical and photocatalytic

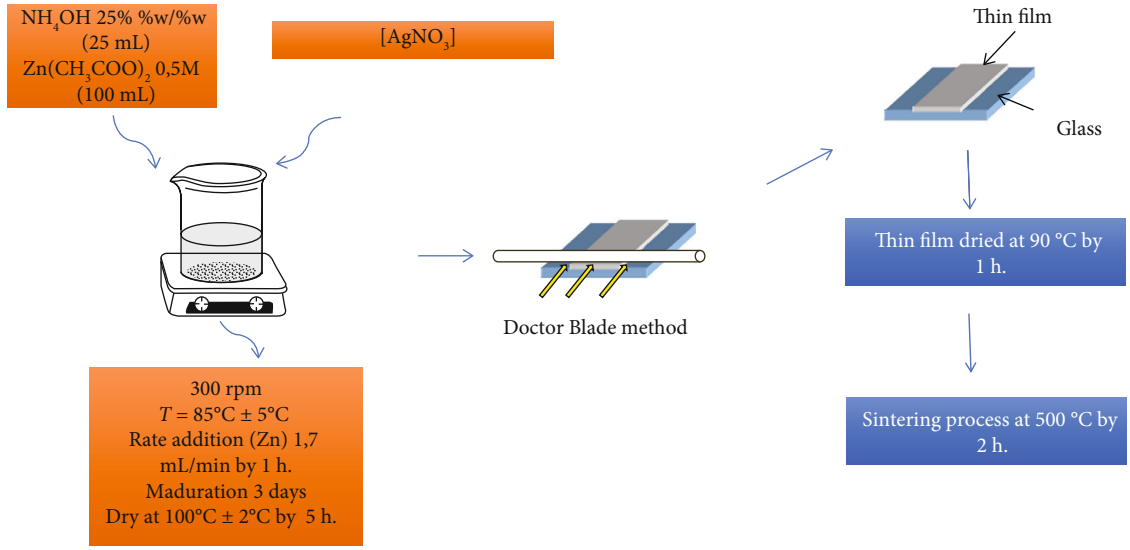

Figure 1: Synthesis procedure for ZnO and Ag-doped ZnO thin films synthesized by the sol-gel method and deposited by the Doctor Blade method [33–35].

properties of ZnO [26–29]. Ag has proved its potential in nanojunction fabrication for photocatalytic applications [30]. Among transition metals, Ag-doped ZnO powders have been successfully prepared using controlled precipitation techniques at low temperature [26].

The insertion of silver into the crystal lattice of ZnO has received great attention for making the catalyst active under visible light. In this regard, Yildirim et al. synthesized silver-doped ZnO and reported that Ag has great affinity in the substitution of Zn^{+2} ions in the semiconductor crystal lattice; this effect caused the inclusion of energetic states within ZnO, which decreased the Fermi level thus modifying the absorption of the semiconductor towards regions farthest away from the electromagnetic spectrum [31]. Additionally, Kakhki et al. reported photocatalytic degradation of toxic organic dyes under various light radiations [32]. The incorporation of Ag into the ZnO structure changes optical absorption towards regions of lower energy, extending the photocatalytic activity towards the visible region of the electromagnetic spectrum. In the present study, Ag-doped ZnO thin films were sensitized and characterized for photocatalytic applications under visible irradiation.

2. Materials and Methods

2.1. Photocatalytic Synthesis and Thin Film Deposition. The amount of 25 mL of ammonium hydroxide (NH_4OH) (25-35% *w*/*w*) reactive grade (Merck) was added to a 250 mL glass beaker; then [$Zn(CH_3COO)_2.2H_2O$] (Merck) 0.500 M was added dropwise at a rate of 1.7 mL·min^{-1} for 1 hour, at a temperature of 85°C under constant agitation at 300 rpm. After that, the suspension stood for three days at room temperature; then, the solid was filtered and dried for 5 hours at 100°C [33, 34]. For the ZnO doping process, a similar procedure was used, as previously described, and during the addition of Zn^{2+} ions, salt [$AgNO_3$] (Merck) was added at 1.0%, 3.0%, and 5.0%. Figure 1 shows the synthesis procedure for ZnO and Ag-doped ZnO.

The thin films were deposited using the Doctor Blade method, and the suspension was placed on a 2 cm high by 2 cm wide glass [35]. The thin films were heated for 30 minutes at 90°C to evaporate the solvent, and finally, the sintering process was performed at 500°C for 2 hours [34]. Figure 1 shows the thin film synthesis procedure used in this study.

2.2. Thin Film Characterization. The Ag content was determined by optical emission spectrometers with inductively coupled plasma (ICP plasma) using a Perkin Elmer Optima 7300DV spectrometer (Supporting Information). The physical chemistry properties of the films were studied by X-ray diffraction, diffuse reflectance spectrophotometry, and Raman spectroscopy assay. X-ray diffraction patterns were obtained using a Shimadzu 6000 diffractometer using Cu Kα radiation ($\lambda = 0.15406$ nm) as an X-ray source with a diffraction angle in the 2θ range (20°-80°). Diffuse reflectance spectra were obtained with a Lambda 4 Perkin-Elmer spectrophotometer equipped with an integration sphere. The compositional properties of the materials were studied by Raman spectroscopy in a DXR device equipped with a 780 nm laser. The morphological properties were studied by scanning electron microscopy (under an excitation energy of 5 and 1 kV). The metallic content of the films was determined by plasma emission spectroscopy using the SM 3120 B technique, EPA 3015A, modified for solids. Finally, XPS measurements were performed on an X-ray photoelectronic spectrometer (NAP-XPS; brand Specs) with a PHOIBOS 150 1D-DLD analyzer, using a monochromatic source of Al-K_α (1486.7 eV, 13 kV, and 100 W) with energy from the 90 eV for the general spectra and 20 eV for the high-resolution spectra. The step was 1 eV for the general spectra and 0.1 eV for the high spectra. A total of 20 measurement cycles were performed for the high-resolution spectra and 3 for the general spectra.

2.3. Photocatalytic Test. Methylene blue (MB) was chosen as the pollutant model in this study. The experiments were carried out in a batch reactor using a LED tape as a source of visible radiation (cold white light 17 watts). To reach adsorption-desorption equilibrium on the catalyst surface, before irradiation, the MB solution was kept in the dark for 90 minutes at 250 rpm. Photodegradation was carried out using 50 mL ± 0.025 mL of a MB solution (10 mg·L^{-1}) saturated with oxygen at pH 7.0. The concentration of dye was determined through the spectrophotometric method (Thermo Scientific, Genesys 10S) using 665 nm as a fixed wavelength, with a calibration curve (correlation coefficient $R = 0.997$) for the use of the Lambert–Beer equation.

2.4. Trapping Experiments. The effect of three different scavengers was studied to find out a possible mechanism for MB photocatalytic degradation and the same concentrations (1.0×10^{-3} M) of isopropyl alcohol (IPA) (OH∗ radical scavengers) [36], parabenzoquinone (PBQ) ($O_2^{\cdot-}$), and potassium iodide (KI) (an h^+ scavenger) [37] were added in separate MB photocatalytic experiments [38, 39].

3. Results and Discussions

3.1. Raman Study. The wurtzite structure of ZnO belongs to the space group C^4_{6v} with two formula units per unit cell, with 8 vibrational modes for ZnO:A_1 ; A_2; B_1; B_2; $2E_1$; and $2E_2$, where modes A_1 and E_1 are polar, showing different frequencies for transverse (TO) and longitudinal (LO) phonons, both modes being Raman and infrared active [40]. Figure 2 shows the Raman spectrum of the ZnO thin films. The peak located at 97.4 cm^{-1} is associated to vibrational mode E_{2L}; the weak signal located at 340 cm^{-1} corresponds to E_{2H}-E_{2L}, and the peaks located at 437.0 cm^{-1} and 581 cm^{-1} correspond to vibrational mode A_1 [41, 42]. The signals located at 274.4 cm^{-1} and 512.6 cm^{-1} do not correspond to the ZnO normal vibrational mode, but these signals have been associated with the presence of defects inside the semiconductor network [43, 44]. For the Ag-doped ZnO films with different silver contents, Figure 2 shows a signal shift located at 581 cm^{-1} towards lower wavenumber values near to 572 cm^{-1} (the signal was expanded and moved approximately 9 cm^{-1} towards lower energy values), and this change can be attributed to the dispersion contributions of the A_{1LO} process outside the Brillouin area. Zeferino et al. reported that such displacement and widening of the signal can be attributable to oxygen vacancies, Zn interstitials, and/or defect complexes in the ZnO network [45].

3.2. XPS Study. The XPS measurements were conducted to verify the surface components and valence states of thin film. Figure 3(a) shows profile XPS spectrum for both ZnO and ZnO:Ag (5%) thin films; the profile of the sample shows the typical signals of binding energy corresponding to Zn, Ag, O, and C elements. The signals located at 1043.4 eV, 1020.5 eV, 139.0 eV, and 88.8 eV correspond to the electronic transitions of Zn $2p_{1/2}$, Zn $2p_{3/2}$, Zn $3s_{1/2}$, and Zn $3p_{3/2}$, respectively [46]. Figure 3(a) also shows an important signal at 532.5 eV; this corresponds to the phototransition O 1 s; the signal located at 285.0 eV corresponds to electronic transition of C 1 s; this signal is typical of atmospheric CO_2 absorbed on the surface. The Ag-doped samples showing the signals at 374.0 eV and 368.0 eV correspond to the electronic transitions of Ag $3d_{3/2}$ and Ag $3d_{3/2}$, respectively (Figure 3(b),

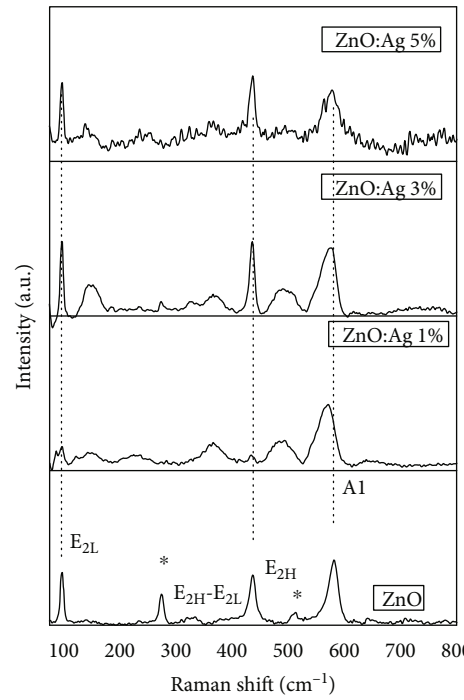

Figure 2: Raman spectrum for both the ZnO and ZnO:Ag thin films. The Raman vibration modes are shown in the figure, where ∗ corresponds to defects inside the ZnO structure.

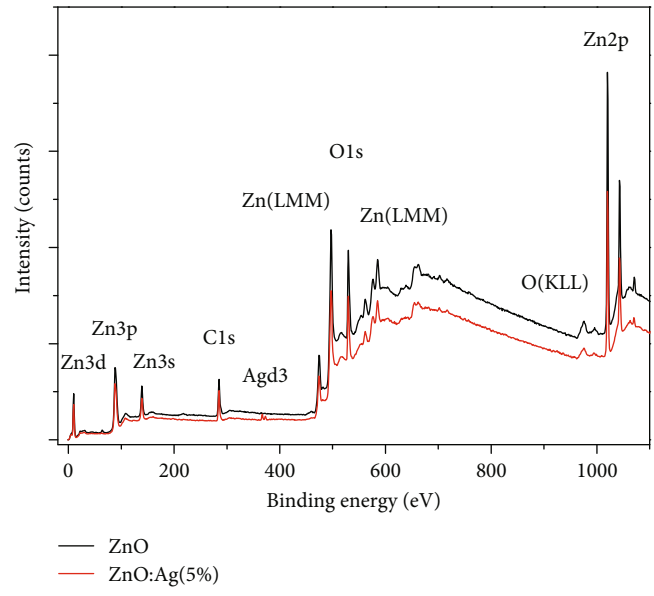

Figure 3: XPS spectrum for both ZnO and ZnO:Ag (5%) thin films.

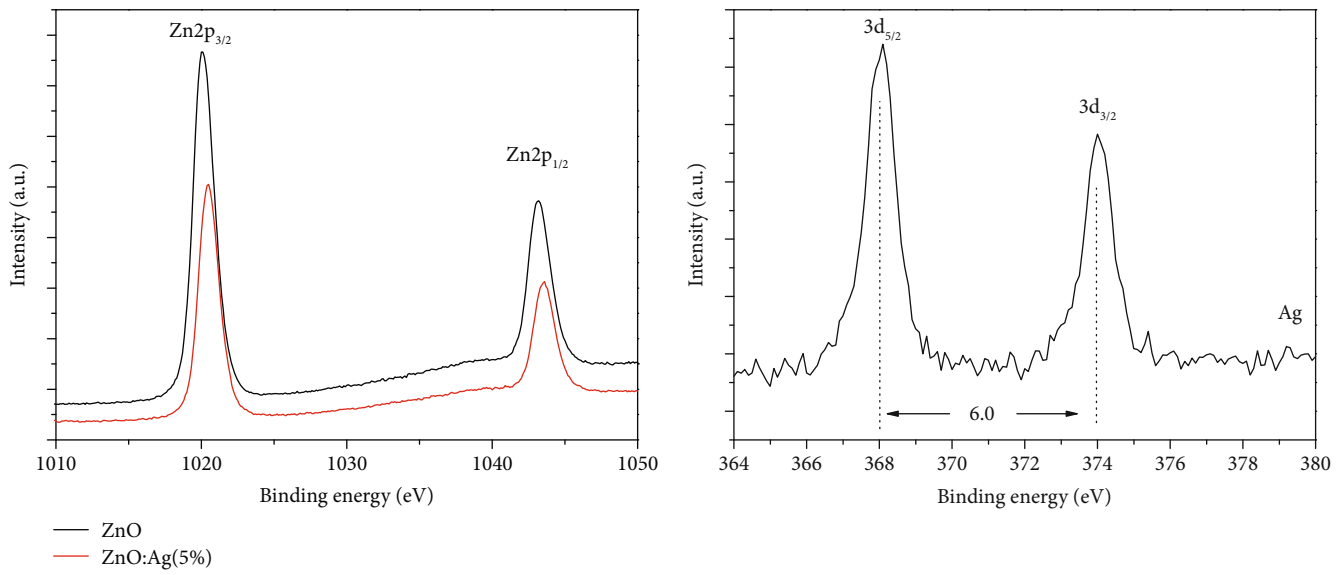

Figure 4: (a) HRXPS Zn 2p spectrum for both ZnO and ZnO:Ag (5%) thin films and (b) HRXPS Ag 3d spectrum for ZnO:Ag (5%) thin films. All binding energies of the XPS spectra are calibrated with reference to the C1s peak at 285 eV.

red line) [47]. Figure 4(a) plots the HRXPS spectrum for $2p_{1/2}$ and Zn $2p_{3/2}$ doublet. Results shows that Zn-2p levels were found to be shifted to higher binding energies after the doping process, the binding energy shift was 0.4 eV (Figure 4(a)), these shifts in the binding energies presumably indicate a change in chemical binding due to dopant atoms, and similar trends were reported by Shin et al. [48] and Lupan et al. [49]. Besides, Figure 4(b) plots the HRXPS spectrum of Ag $3d_{5/2}$ and Ag $3d_{3/2}$ double peaks, which are centered at 368.0 and 374.0 eV, respectively, and the splitting of the 3d doublet was 6.0 eV suggesting that silver was in metallic nature into ZnO thin films [50, 51]. Thomas et al. and Khosravi-Gandomani et al. have revealed the presence of two different components, which could be attributed to either metallic Ag or Ag_2O and to an Ag-Zn-O ternary compound [52, 53]. Thongsuriwong et al. observed a similar behavior in Ag 3d spectra for Ag-doped ZnO thin films [54].

3.3. Structural Study. Figure 5 shows the X-ray diffraction pattern for the ZnO and doped ZnO thin films. The ZnO thin film pattern shows typical signals for the hexagonal Wurtzite phase (JCPDS No. 36-1451), with the thin films being polycrystalline and the sample presenting a preferential growth plane at $2\theta = 36.27$ corresponding to the crystalline plane (101)—these results agree with those of other reports [55]. After the doping process, the diffraction patterns preserved signals of the wurtzite ZnO structure but there was a change in the intensity of the main diffraction signal, corresponding to the plane diffraction (101). This behavior is the result of the Ag doping process, and besides, the change in the intensities of the diffraction signals was associated to changes in grain size due to network defects or oxygen vacancies [56, 57]. Finally, based in Raman spectroscopy, the XPS, and the structural characterization, these results suggest that metallic Ag was incorporated into the ZnO.

3.4. Morphological Study. Figure 6 shows AFM images for the ZnO and ZnO:Ag thin films, and Table 1 shows the roughness and grain size values for the thin films. The results show that ZnO films are composed of aggregates with size in a nanoscale range. The surface properties (roughness and grain size) of the ZnO thin films are affected by the doping process, in which both roughness and grain size of the films are greater than the roughness of the Ag-doped ZnO films. The average size of the grains is smaller than 200 nm, and the grain size changes in a range of 120 nm to 190 nm—the thin film grain size decreased after the doping process as a result of the incorporation Ag^0 as a dopant into the ZnO crystal lattice [58].

3.5. Optical Study. Figure 7(a) shows the diffuse reflectance spectrum for both the ZnO and the Ag-doped ZnO thin films. The results show that the ZnO thin films had a high reflectance of approximately 70% after 370 nm. In the visible region, reflectance changes as a function of the doping metal load; reflectance decreases as the metal load increases—this observation is general for all thin films. Reports in the literature indicate that the incorporation of dopant metal into the ZnO crystal lattice decreases the band gap (Eg). The Eg value is determined using the Kubelka-Munk function [59]:

$$F(R_\infty) = \frac{(1 - R_\infty)^2}{2\,R_\infty}, \quad (1)$$

where R_∞ is the material reflectance value and $F(R_\infty)$ represents the ratio between the absorption and the scattering coefficients; $F(R_\infty)$ is proportional to the absorption

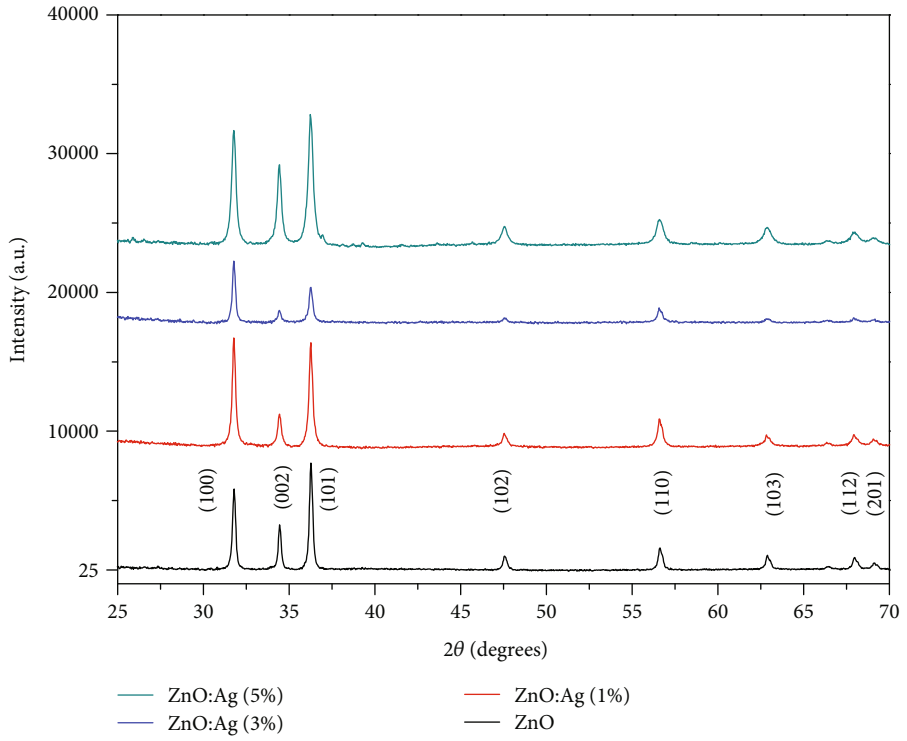

Figure 5: X-ray diffraction patterns for both ZnO and ZnO:Ag thin films.

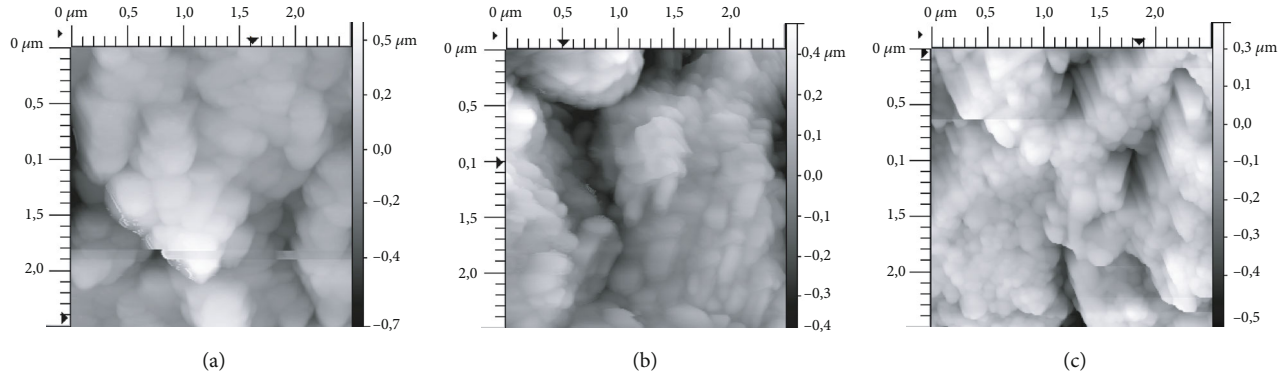

Figure 6: AFM images for (a) ZnO, (b) ZnO:Ag 1%, and (c) ZnO:Ag 5% thin films.

Table 1: Roughness and grain size of TiO_2 and TiO_2/sensitizer thin films.

Thin films	Grain size (nm)	Roughness (nm)
ZnO	190	18.4
ZnO:Ag (1%)	130	25.7
ZnO:Ag (5%)	120	36.6

constant of the material, an indication of the sample absorbance at a particular wavelength. From Equation (1) and the curves shown in Figure 5(a), an analogue to Tauc plots $(F(R_\infty)h\nu)^{1/2}$ against photon energy can be constructed, according to [60]

$$(F(R_\infty)h\nu)^{1/2} = A(h\nu - \mathrm{Eg}). \quad (2)$$

Figure 5(b) shows plots of $(F(R_\infty)h\nu)^{1/2}$ versus $(h\nu)$ for the diffuse reflectance spectra shown in Figure 5(a). The optical band gap of the films was determined by extrapolating the linear portion of the graph onto the x-axis [61]. Table 2 lists the optical properties for the thin films.

Figure 7(b) shows that the ZnO thin films had a band gap value of 3.22 eV, a value that is lower than the Eg value reported for ZnO (3.37 eV). This result is associated to defects or oxygen vacancies inside the ZnO structure. During ZnO synthesis, oxygen vacancies are the most favorable defects to form. However, Srikant et al. reported apparent band gaps for ZnO of 3.1 eV and 3.2 eV due to the existence of a valence band-donor level transition at ~3.15 eV, which can dominate the absorption spectrum [62, 63]. For the doped ZnO thin films, the inclusion of Ag modified the semiconductor absorption towards lower energy regions of the electromagnetic spectrum (Table 2). This is associated to

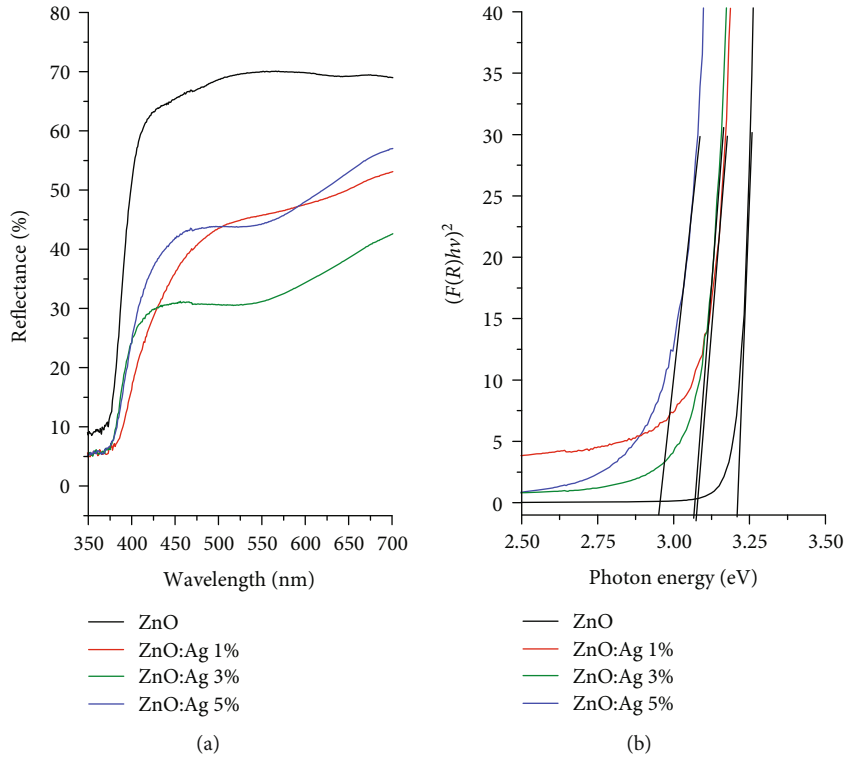

Figure 7: (a) Reflectance diffuse spectra for both ZnO and ZnO:Ag thin films. (b) Kubelka-Munk plots and band gap energy estimation for both ZnO and ZnO:Ag thin films.

Table 2: Optical and kinetic results for both ZnO:Cu and ZnO:Co thin films.

Thin film	Band gap (eV)	Degradation (%)	*Ratio $D_{Ag:ZnO}/D_{ZnO}$	$k_{app} \times 10^{-3}$ (min^{-1})
ZnO	3.22	2.7	1.0	0.2
ZnO:Ag 1%	2.95	30.8	13.5	2.7
ZnO:Ag 3%	3.12	37.5	17	3.4
ZnO:Ag 5%	3.10	44.8	20.5	4.1

*Degradation $(\%)_{ZnO:Ag}$/degradation $(\%)_{ZnO}$.

reduction of the ZnO Fermi level by generation of intragap states, where these new levels modified the absorption of the semiconductor towards regions of lower energy of the electromagnetic spectrum (ZnO:Ag 1%). This result corresponds to results of other reports [64]; however, for films with a higher percentage of Ag doping (2% and 5%), the optical band gap was bigger. Shinde et al. reported that when Ag doping exceeds the doping load, the electron mobility is diminished due to deformation of the ZnO film structure, caused by the greater ionic radius of Ag (0.115 nm) with respect to Zn (0.074 nm), which would prevent the optical response of the material from being improved [65].

3.6. Photocatalytic Study. Figure 8 indicates that the doping process had a positive effect on the photocatalytic activity of ZnO under visible irradiation; all the doped samples had a greater photocatalytic activity than that of the ZnO films. The degradation percentages of all the samples are

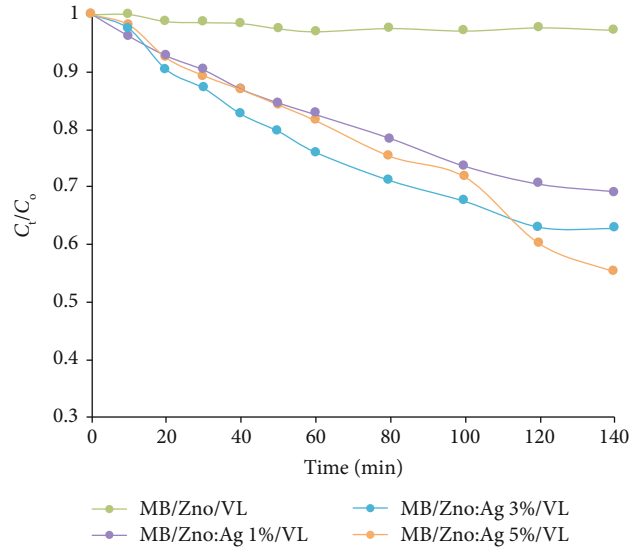

Figure 8: MB photocatalytic degradation for both ZnO and ZnO:Ag thin films after 140 min under visible light (VL) irradiation.

listed in Table 2. The Ag-doped ZnO thin films (5%) showed the highest photocatalytic activity. The improvement in the catalytic activity could be attributed to the fact that the grain size was smaller than the ZnO thin films, which favored having an effective surface with larger sites available for adsorption and, besides that (Table 1), Ag-doped ZnO thin films had a smaller band gap value (Table 2). In addition,

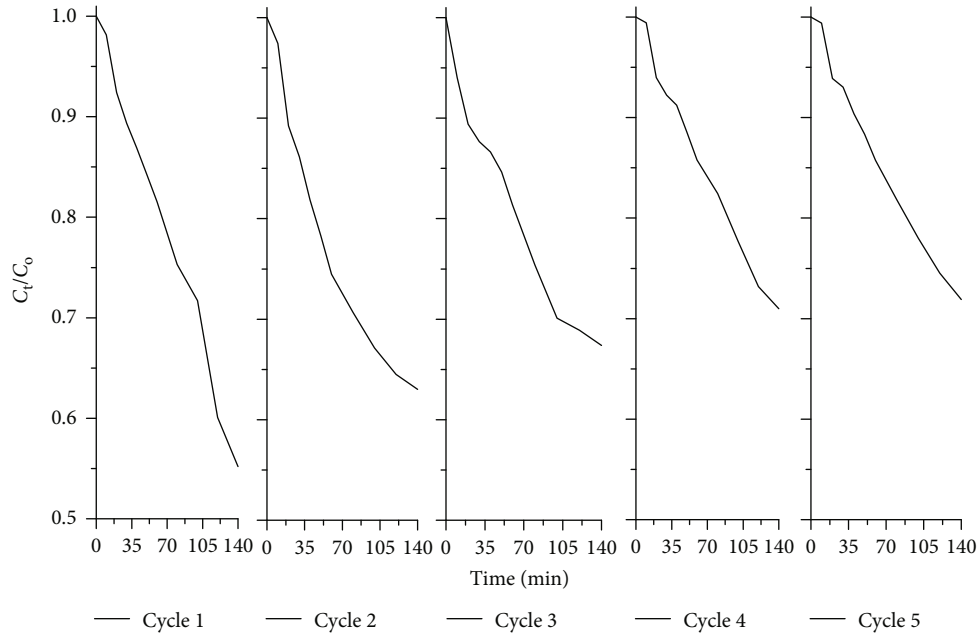

Figure 9: Recycling test for MB photocatalytic degradation under visible irradiation on ZnO:Ag (5%) thin films.

silver acts as an electron acceptor, favoring p-type conduction and decreasing the recombination of charge carriers [45]. The photodegradation kinetics of MB was studied using the Langmuir-Hinshelwood kinetic expression:

$$v = -\frac{d[\mathrm{AM}]}{dt} = \frac{k * K[\mathrm{BM}]}{1 + K[\mathrm{BM}]}, \tag{3}$$

where v is the dye mineralization rate, K is the speed constant, [MB] is the concentration of methylene blue, and k is the adsorption coefficient. Equation (3) can be explicitly resolved for (t) to use discrete changes in [MB] from the initial concentration to a zero-reference point. In the present case, an apparent first-order model can be supposed:

$$v = -\frac{d[\mathrm{AM}]}{dt} = k_{\mathrm{app}}[\mathrm{AM}] = kK[\mathrm{AM}],$$
$$[\mathrm{AM}] = [\mathrm{AM}]_o e^{k_{\mathrm{app}}t}, \tag{4}$$

where time (t) is expressed in minutes and k_{app} $(k * K)$ is the apparent reaction speed constant (min^{-1}). The k_{app} values for synthesized catalysts are listed in Table 2. The results show that the doping process increased the speed constant from a value of 2.0×10^{-4} min^{-1} for the unmodified ZnO thin films to a value of 4.1×10^{-3} min^{-1} for ZnO:Ag 5%—in the best case, the speed degradation is 20.5 times higher than unmodified ZnO. Both the combined effect of the band gap and grain size reduction by the doping process explain the increase of the MB degradation percentage under visible light irradiation.

Jayswal and Moirangthem reported a k_{app} value of 5.9×10^{-3} min^{-1} for photocatalytic degradation of methyl orange after 150 min under visible light irradiation using an SnS/ZnO heterostructure as a photocatalyst [66]. In another study, Park et al. reported a k_{app} value of 2.7×10^{-3} min^{-1} for photocatalytic degradation of 2,4-dinitrophenol after 140 min under visible light irradiation using functionalized zinc oxide tetrapods as photocatalysts [67]. Türkyilmaz et al. reported a k_{app} value of 7.5×10^{-3} min^{-1} for visible light photocatalytic degradation of tartrazine after 150 min using Fe-doped ZnO as photocatalysts [22]. Kuriakose et al. reported a k_{app} value of 2.2×10^{-2} min^{-1} for MB photocatalytic degradation after 30 min under visible light irradiation using Cu-doped ZnO powders as photocatalyst [68]. Although the best k_{app} value reported in Table 2 is lower, several practical problems arise from the use of powder during the photocatalytic process: (a) separation of insoluble catalyst from suspension is harder and slower than thin films, (b) suspended particles tend to aggregate at high concentrations, and (c) suspensions are not easy to apply in continuous flow systems; these drawbacks increase the costs of practical applications of photocatalysis [69]. The immobilization of ZnO through thin films provides an advantage over the drawbacks of powder suspensions.

Besides, the study determined the recyclability of the best thin film for MB photodegradation under visible light. Figure 9 shows the recycling test for of the ZnO:Ag (5%) thin films. The thin films showed suitable stability after 5 repetitive photocatalysis tests using the same thin film, after the first cycle the photodegradation yield was reduced (17%) and in the 5^{th} cycle the photodegradation yield was reduced (40%). Finally, recycling results show that after the doping process, photostability is conserved, indicating that ZnO:Ag (5%) thin films are suitable as reusable photocatalysts for sunlight-driven photocatalytic degradation after 5 cycles.

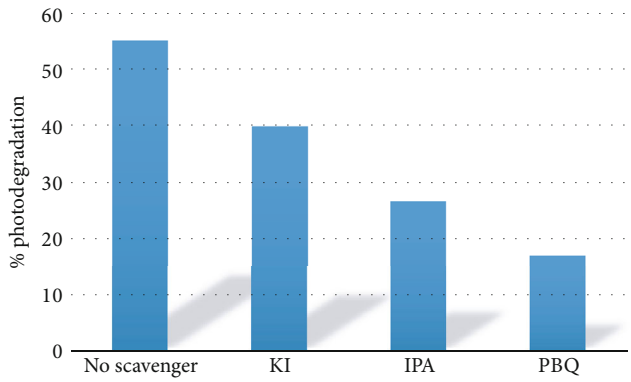

Figure 10: Result of MB photodegradation in the presence of reactive oxygen species scavengers, after 120 minutes under visible irradiation on ZnO:Ag (5%) thin films.

3.7. Photodegradation Mechanism. Figure 10 compares the results of trapping experiments in the presence of different reactive oxygen species scavengers under visible irradiation on ZnO:Ag (5%) thin films. The results show that the effect of the KI scavenger decreases about 27% the photodegradation yield, that of the IPA scavenger decreases about 51% the photodegradation yield, and that of the PBQ scavenger decreases about 70% the photodegradation yield. The biggest decrease in photocatalytic yield was reported for the addition of PBQ, suggesting that $O_2^{\cdot-}$ could be the main reactive oxygen species (ROS) driving the photocatalytic process. After irradiation, $O_2^{\cdot-}$ can be generated according to

$$\mathrm{ZnO:Ag} + h\nu_{(E>\mathrm{Eg})} \longrightarrow \mathrm{ZnO:Ag}\left(\frac{h_{\mathrm{iel}}^{+}}{e_{\mathrm{cb}}^{-}}\right), \quad (5)$$

$$\left(e_{\mathrm{cb}}^{-}\right) + \mathrm{O}_{2(\mathrm{ad})} \longrightarrow {\mathrm{O}_2^{\cdot-}}_{(\mathrm{ad})}, \quad (6)$$

$${\mathrm{O}_2^{\cdot-}}_{(\mathrm{ad})} + \mathrm{MB}_{(\mathrm{ad})} \longrightarrow {\mathrm{MB}^{\cdot+}}_{(\mathrm{ad})} \longrightarrow \text{degradation products}, \quad (7)$$

where cb is the conduction bands of the semiconductor and iel is the intermediate energy levels generated after doping process. Under correct electromagnetic irradiation ($E_{h\nu} \geq \mathrm{Eg}$), the semiconductor absorbs this radiation and one electron can be excited from the doping donor level to cd of the semiconductor (equation (5)). In solution, the oxygen molecules adsorbed on the semiconductor surface prevent recombination by trapping electrons and this generates superoxide radical anions (equation (6)) [70, 71].

Methylene blue photodegradation proceeds through both parallel and consecutive reactions, as superoxide radical anions can react directly with MB (equation (7)). The fact that the KI scavenger decreases about 19% the photodegradation yield indicates that holes (h^+) can be produced in minor proportion after visible absorption, and the redox potential of holes is thermodynamically suitable to oxidize almost any organic molecule. Charge carrier trapping would suppress the recombination and increase the lifetime of the separated electron and hole; other factors such as surface area, crystallinity, and trap density can affect the photocatalytic performance of the semiconductor [70–72]:

$$\left(h_{\mathrm{vb}}^{+}\right) + \mathrm{H_2O_{a(d)}} \longrightarrow {\mathrm{OH}^{\cdot}}_{(\mathrm{ad})} + \mathrm{H}^{+}, \quad (8)$$

$$\left(h^{+}\right) + {\mathrm{OH}^{-}}_{(\mathrm{ad})} \longrightarrow {\mathrm{OH}^{\cdot}}_{(\mathrm{ad})}, \quad (9)$$

$$\left(h^{+}\right) + \mathrm{MB}_{(\mathrm{ad})} \longrightarrow {\mathrm{MB}^{\cdot+}}_{(\mathrm{ad})} \longrightarrow \text{degradation products}, \quad (10)$$

$${\mathrm{OH}^{\cdot}}_{(\mathrm{ad})} + \mathrm{MB}_{(\mathrm{ad})} \longrightarrow {\mathrm{MB}^{\cdot+}}_{(\mathrm{ad})} \longrightarrow \text{degradation products}. \quad (11)$$

Furthermore, oxidation by holes yields more hydroxyl radical molecules (equations (8) and (9)). Given that hydroxyl radicals are powerful oxidizing species, they are considered important species in the photocatalytic processes. Finally, MB photodegradation can proceed through both parallel and consecutive reactions (equations (10) and (11)).

4. Conclusions

This study synthesized and characterized Ag-doped ZnO thin films. The spectroscopic, morphological, and structural characterization of the composites was presented in detail. All results corroborated the doping process; the red shift in the band gap values was detected after the doping process, from 3.22 eV (ZnO) to 2.95 eV (ZnO:Ag 1%). XPS indicates that silver was incorporated as Ag^0 inside ZnO after the doping process. Besides, the photocatalysis test indicated that doped ZnO thin films exhibited higher photocatalytic activity than ZnO thin films, a behavior that was attributed to (i) intraband transitions due to dopant insertion inside ZnO and (ii) reduction in grain size. Trapping experiments reveled that $O_2^{\cdot-}$ was the main ROS generated after visible light irradiation on ZnO:Ag (5%) thin films. Finally, in the best case, the photodegradation percentage for ZnO:Ag (5%) was 16.5 times higher than that for the unmodified ZnO.

Data Availability

The data used to support the findings of this study can be made available by the corresponding author upon request.

Conflicts of Interest

The authors declare that there are no conflicts of interest.

Acknowledgments

This study was supported by Universidad del Atlántico (the first internal call granting financial support for the development of degree papers on formative research—undergraduate and postgraduate levels). The authors thank Universidad del Atlántico for the financial support.

Supplementary Materials

Figure S1: ICP calibration curve for Ag content. (equipment: ICP-OES ICAP SERIE 7200, Thermo Scientific; method SM 3120 B, EPA 3015A adapted for solids). Table S1: results of ICP for Ag content in Ag-doped ZnO thin films. *(Supplementary Materials)*

References

[1] M. A. Mohd Adnan, N. Muhd Julkapli, M. N. I. Amir, and A. Maamor, "Effect on different TiO_2 photocatalyst supports on photodecolorization of synthetic dyes: a review," *International Journal of Environmental Science and Technology*, vol. 16, no. 1, pp. 547–566, 2019.

[2] J. Bedia, V. Muelas-Ramos, M. Peñas-Garzón, A. Gómez-Avilés, J. J. Rodríguez, and C. Belver, "A review on the synthesis and characterization of metal organic frameworks for photocatalytic water purification," *Catalysts*, vol. 9, no. 1, p. 52, 2019.

[3] D. Spasiano, R. Marotta, S. Malato, P. Fernandez-Ibañez, and I. Di Somma, "Solar photocatalysis: materials, reactors, some commercial, and pre- industrialized applications. A comprehensive approach," *Applied Catalysis B: Environmental*, vol. 170-171, pp. 90–123, 2015.

[4] A. G. Gutierrez-Mata, S. Velazquez-Martínez, A. Álvarez-Gallegos et al., "Recent overview of solar photocatalysis and solar photo-Fenton processes for wastewater treatment," *International Journal of Photoenergy*, vol. 2017, Article ID 8528063, 27 pages, 2017.

[5] K. Siwińska-Stefańska, A. Kubiak, A. Piasecki et al., "TiO_2-ZnO binary oxide systems: comprehensive characterization and tests of photocatalytic activity," *Materials*, vol. 11, no. 5, p. 841, 2018.

[6] C. Yuan, H. B. Wu, Y. Xie, and X. W. D. Lou, "Mixed transition-metal oxides: design, synthesis, and energy-related applications," *Angewandte Chemie International Edition*, vol. 53, no. 6, pp. 1488–1504, 2014.

[7] A. Das, P. Malakar, and R. G. Nair, "Engineering of ZnO nanostructures for efficient solar photocatalysis," *Materials Letters*, vol. 219, pp. 76–80, 2018.

[8] M. Yin, Z. Li, J. Kou, and Z. Zou, "Mechanism investigation of visible light-induced degradation in a heterogeneous TiO_2/eosin Y/rhodamine B system," *Environmental Science & Technology*, vol. 43, no. 21, pp. 8361–8366, 2009.

[9] W. Vallejo, C. Diaz-Uribe, and Á. Cantillo, "Methylene blue photocatalytic degradation under visible irradiation on TiO_2 thin films sensitized with Cu and Zn tetracarboxy- phthalocyanines," *Journal of Photochemistry and Photobiology A: Chemistry*, vol. 299, pp. 80–86, 2015.

[10] W. Vallejo, A. Rueda, C. Díaz-Uribe, C. Grande, and P. Quintana, "Photocatalytic activity of graphene oxide–TiO_2thin films sensitized by natural dyes extracted from *Bactris guineensis*," *Royal Society Open Science*, vol. 6, no. 3, p. 181824, 2019.

[11] C. Díaz-Uribe, W. Vallejo, K. Campos et al., "Improvement of the photocatalytic activity of TiO_2 using Colombian Caribbean species (*Syzygium cumini*) as natural sensitizers: experimental and theoretical studies," *Dyes and Pigments*, vol. 150, pp. 370–376, 2018.

[12] Ritika, M. Kaur, A. Umar et al., "Rapid solar-light driven superior photocatalytic degradation of methylene blue using MoS_2-ZnO heterostructure nanorods photocatalyst," *Materials*, vol. 11, no. 11, p. 2254, 2018.

[13] J. Zhong, J. Li, J. Zeng et al., "Enhanced photocatalytic activity of In_2O_3-decorated TiO_2," *Applied Physics A*, vol. 115, no. 4, pp. 1231–1238, 2014.

[14] W. Vallejo, C. Díaz-Uribe, and K. Rios, "Methylene blue photocatalytic degradation under visible irradiation on In_2S_3 synthesized by chemical bath deposition," *Advances in Physical Chemistry*, vol. 2017, Article ID 6358601, 5 pages, 2017.

[15] B. Subash, B. Krishnakumar, M. Swaminathan, and M. Shanthi, "Highly efficient, solar active, and reusable photocatalyst: Zr-loaded ag–ZnO for reactive red 120 dye degradation with synergistic effect and dye-sensitized mechanism," *Langmuir*, vol. 29, no. 3, pp. 939–949, 2013.

[16] H. Aby, A. Kshirsagar, and P. K. Khanna, "Plasmon mediated photocatalysis by solar active Ag/ZnO nanostructures: degradation of organic pollutants in aqueous conditions," *Journal of Materials Science and Nanotechnology*, vol. 4, no. 1, p. 103, 2016.

[17] C. Díaz-Uribe, J. Viloria, L. Cervantes et al., "Photocatalytic activity of Ag-TiO_2 composites deposited by photoreduction under UV irradiation," *International Journal of Photoenergy*, vol. 2018, Article ID 6080432, 8 pages, 2018.

[18] L. Chen, T. ThanhThuy Tran, C.'a. Huang, J. Li, L. Yuan, and Q. Cai, "Synthesis and photocatalytic application of Au/Ag nanoparticle-sensitized ZnO films," *Applied Surface Science*, vol. 273, pp. 82–88, 2013.

[19] J. Schumann, M. Eichelbaum, T. Lunkenbein et al., "Promoting strong metal support interaction: doping ZnO for enhanced activity of Cu/ZnO:M (M = Al, Ga, Mg) catalysts," *ACS Catalysis*, vol. 5, no. 6, pp. 3260–3270, 2015.

[20] V. Kumari, A. Mittal, J. Jindal, S. Yadav, and N. Kumar, "S-, N- and C-doped ZnO as semiconductor photocatalysts: a review," *Frontiers of Materials Science*, vol. 13, no. 1, pp. 1–22, 2019.

[21] T. C. Bharat, Shubham, S. Mondal, H. S. Gupta, P. K. Singh, and A. K. Das, "Synthesis of doped zinc oxide nanoparticles: a review," *Materials Today: Proceedings*, vol. 11, pp. 767–775, 2019.

[22] Ş. Ş. Türkyılmaz, N. Güy, and M. Özacar, "Photocatalytic efficiencies of Ni, Mn, Fe and Ag doped ZnO nanostructures synthesized by hydrothermal method: the synergistic/antagonistic effect between ZnO and metals," *Journal of Photochemistry and Photobiology A: Chemistry*, vol. 341, pp. 39–50, 2017.

[23] B. M. Rajbongshi and S. K. Samdarshi, "Cobalt-doped zincblende–wurtzite mixed-phase ZnO photocatalyst nanoparticles with high activity in visible spectrum," *Applied Catalysis B: Environmental*, vol. 144, pp. 435–441, 2014.

[24] K. Umar, A. Aris, T. Parveen et al., "Synthesis, characterization of Mo and Mn doped ZnO and their photocatalytic activity for the decolorization of two different chromophoric dyes," *Applied Catalysis A: General*, vol. 505, pp. 507–514, 2015.

[25] M. K. Lima, D. M. Fernandes, M. F. Silva et al., "Co-doped ZnO nanoparticles synthesized by an adapted sol–gel method: effects on the structural, optical, photocatalytic and antibacterial properties," *Journal of Sol-Gel Science and Technology*, vol. 72, no. 2, pp. 301–309, 2014.

[26] H. Bouzid, M. Faisal, F. A. Harraz, S. A. Al-Sayari, and A. A. Ismail, "Synthesis of mesoporous Ag/ZnO nanocrystals with enhanced photocatalytic activity," *Catalysis Today*, vol. 252, pp. 20–26, 2015.

[27] O. Altintas Yildirim, H. Arslan, and S. Sönmezoğlu, "Facile synthesis of cobalt-doped zinc oxide thin films for highly

efficient visible light photocatalysts," *Applied Surface Science*, vol. 390, pp. 111–121, 2016.

[28] M. Ahmad, E. Ahmed, W. Ahmed, A. Elhissi, Z. L. Hong, and N. R. Khalid, "Enhancing visible light responsive photocatalytic activity by decorating Mn- doped ZnO nanoparticles on graphene," *Ceramics International*, vol. 40, no. 7, pp. 10085–10097, 2014.

[29] İ. Polat, S. Yılmaz, İ. Altın, E. Bacaksız, and M. Sökmen, "The influence of Cu-doping on structural, optical and photocatalytic properties of ZnO nanorods," *Materials Chemistry and Physics*, vol. 148, no. 3, pp. 528–532, 2014.

[30] L. S. Zhang, K. H. Wong, H. Y. Yip et al., "Effective photocatalytic disinfection ofE. coliK-12 using AgBr–Ag–Bi2WO6nanojunction system irradiated by visible light: the role of diffusing hydroxyl radicals," *Environmental Science & Technology*, vol. 44, no. 4, pp. 1392–1398, 2010.

[31] Ö. A. Yıldırım, H. E. Unalan, and C. Durucan, "Highly efficient room temperature synthesis of silver-doped zinc oxide (ZnO:Ag) nanoparticles: structural, optical, and photocatalytic properties," *Journal of the American Ceramic Society*, vol. 96, no. 3, pp. 766–773, 2013.

[32] R. Mohammadzadeh Kakhki, R. Tayebee, and F. Ahsani, "New and highly efficient Ag doped ZnO visible nano photocatalyst for removing of methylene blue," *Journal of Materials Science: Materials in Electronics*, vol. 28, no. 8, pp. 5941–5952, 2017.

[33] H. R. L. J. A. Pérez, J. L. Gallego, and W. S. Roman, "Zinc oxide nanostructured thin films," in *Scientia et Technica Año XIV, No. 39*, vol. 39, pp. 416–421, Universidad Tecnológica de Pereira, 2008, https://revistas.utp.edu.co/index.php/revistaciencia/article/view/3261.

[34] D. Ramírez Vinasco, L. P. Vera, and R. L. Henry, "Zn1-xMnxO thin films," in *Scientia et Technica Año XV, No 41*, vol. 41, pp. 273–278, Universidad Tecnológica de Pereira, 2009, July 2019, https://revistas.utp.edu.co/index.php/revistaciencia/article/view/2951.

[35] C. Quiñones, J. Ayala, and W. Vallejo, "Methylene blue photoelectrodegradation under UV irradiation on Au/Pd-modified TiO_2 films," *Applied Surface Science*, vol. 257, no. 2, pp. 367–371, 2010.

[36] F. Grieser, "Free radical formation and scavenging by solutes in the sonolysis of aqueous solutions," in *Proceedings of Meetings on Acoustics*, vol. 19, p. 45093, Montreal, Canada, 2013.

[37] T. M. El-Morsi, W. R. Budakowski, A. S. Abd-El-Aziz, and K. J. Friesen, "Photocatalytic degradation of 1,10-dichlorodecane in aqueous suspensions of TiO_2: a reaction of adsorbed chlorinated alkane with surface hydroxyl radicals," *Environmental Science & Technology*, vol. 34, no. 6, pp. 1018–1022, 2000.

[38] M. Pelaez, P. Falaras, V. Likodimos et al., "Use of selected scavengers for the determination of NF- TiO_2 reactive oxygen species during the degradation of microcystin-LR under visible light irradiation," *Journal of Molecular Catalysis A: Chemical*, vol. 425, no. 0, pp. 183–189, 2016.

[39] S. Kumar, S. Pal, J. Kuntail, A. KumarDe, and I. Sinha, "Construction of a visible light Z-scheme photocatalyst: curcumin functionalized Cu_2O/Ag nanocomposites," *ChemistrySelect*, vol. 4, no. 36, pp. 10709–10718, 2019.

[40] M. Samadi, M. Zirak, A. Naseri, E. Khorashadizade, and A. Z. Moshfegh, "Recent progress on doped ZnO nanostructures for visible-light photocatalysis," *Thin Solid Films*, vol. 605, pp. 2–19, 2016.

[41] J. M. Calleja and M. Cardona, "Resonant Raman scattering in ZnO," *Physical Review B*, vol. 16, no. 8, pp. 3753–3761, 1977.

[42] R. Cuscó, E. Alarcón-Lladó, J. Ibáñez et al., "Temperature dependence of Raman scattering in ZnO," *Physical Review B*, vol. 75, no. 16, p. 165202, 2007.

[43] J. Sann, J. Stehr, A. Hofstaetter et al., "Zn interstitial related donors in ammonia-treated ZnO powders," *Physical Review B*, vol. 76, no. 19, article 195203, 2007.

[44] F. Friedrich and N. H. Nickel, "Resonant Raman scattering in hydrogen and nitrogen doped ZnO," *Applied Physics Letters*, vol. 91, no. 11, article 111903, 2007.

[45] R. S. Zeferino, M. B. Flores, and U. Pal, "Photoluminescence and Raman scattering in Ag-doped ZnO nanoparticles," *Journal of Applied Physics*, vol. 109, no. 1, article 014308, 2011.

[46] M. Kwoka, B. Lyson-Sypien, A. Kulis et al., "Surface properties of nanostructured, porous ZnO thin films prepared by direct current reactive magnetron sputtering," *Materials*, vol. 11, no. 1, p. 131, 2018.

[47] Y. Chen, W. H. Tse, L. Chen, and J. Zhang, "Ag nanoparticles-decorated ZnO nanorod array on a mechanical flexible substrate with enhanced optical and antimicrobial properties," *Nanoscale Research Letters*, vol. 10, no. 1, p. 106, 2015.

[48] M. H. Shin, M. S. Park, S. H. Jung, J. H. Boo, and N. E. Lee, "Effect of doping elements on ZnO etching characteristics with CH_4/H_2/Ar plasma," *Thin Solid Films*, vol. 515, no. 12, pp. 4950–4954, 2007.

[49] O. Lupan, L. Chow, L. K. Ono et al., "Synthesis and characterization of Ag- or Sb-doped ZnO nanorods by a facile hydrothermal route," *Journal of Physical Chemistry C*, vol. 114, no. 29, pp. 12401–12408, 2010.

[50] M. Wu, B. Yang, Y. Lv et al., "Efficient one-pot synthesis of Ag nanoparticles loaded on N-doped multiphase TiO_2 hollow nanorod arrays with enhanced photocatalytic activity," *Applied Surface Science*, vol. 256, no. 23, pp. 7125–7130, 2010.

[51] Y. Ao, J. Xu, D. Fu, and C. Yuan, "Preparation of Ag-doped mesoporous titania and its enhanced photocatalytic activity under UV light irradiation," *Journal of Physics and Chemistry of Solids*, vol. 69, no. 11, pp. 2660–2664, 2008.

[52] M. A. Thomas, W. W. Sun, and J. B. Cui, "Mechanism of Ag doping in ZnO nanowires by electrodeposition: experimental and theoretical insights," *Journal of Physical Chemistry C*, vol. 116, no. 10, pp. 6383–6391, 2012.

[53] S. Khosravi-Gandomani, R. Yousefi, F. Jamali-Sheini, and N. M. Huang, "Optical and electrical properties of p -type Ag-doped ZnO nanostructures," *Ceramics International*, vol. 40, no. 6, pp. 7957–7963, 2014.

[54] K. Thongsuriwong, P. Amornpitoksuk, and S. Suwanboon, "Photocatalytic and antibacterial activities of Ag-doped ZnO thin films prepared by a sol-gel dip-coating method," *Journal of Sol-Gel Science and Technology*, vol. 62, no. 3, pp. 304–312, 2012.

[55] E. Muchuweni, T. S. Sathiaraj, and H. Nyakotyo, "Synthesis and characterization of zinc oxide thin films for optoelectronic applications," *Heliyon*, vol. 3, no. 4, article e00285, 2017.

[56] B. D. Yuhas, D. O. Zitoun, P. J. Pauzauskie, R. He, and P. Yang, "Transition-metal doped zinc oxide nanowires," *Angewandte Chemie*, vol. 118, no. 3, pp. 434–437, 2006.

[57] X. Wang, L. Sø, R. Su et al., "The influence of crystallite size and crystallinity of anatase nanoparticles on the photodegradation of phenol," *Journal of Catalysis*, vol. 310, pp. 100–108, 2014.

[58] S. Bai, J. Hu, D. Li, R. Luo, A. Chen, and C. C. Liu, "Quantum-sized ZnO nanoparticles: synthesis, characterization and sensing properties for NO_2," *Journal of Materials Chemistry*, vol. 21, no. 33, p. 12288, 2011.

[59] E. L. Simmons, "Relation of the diffuse reflectance remission function to the fundamental optical parameters," *Optica Acta: International Journal of Optics*, vol. 19, no. 10, pp. 845–851, 1972.

[60] B. D. Viezbicke, S. Patel, B. E. Davis, and D. P. Birnie III, "Evaluation of the Tauc method for optical absorption edge determination: ZnO thin films as a model system," *Physica Status Solidi (b)*, vol. 252, no. 8, pp. 1700–1710, 2015.

[61] M. Pal, U. Pal, J. M. G. Y. Jiménez, and F. Pérez-Rodríguez, "Effects of crystallization and dopant concentration on the emission behavior of TiO_2:Eu nanophosphors," *Nanoscale Research Letters*, vol. 7, no. 1, p. 1, 2012.

[62] V. Srikant and D. R. Clarke, "On the optical band gap of zinc oxide," *Journal of Applied Physics*, vol. 83, no. 10, pp. 5447–5451, 1998.

[63] N. El-Atab, F. Chowdhury, T. G. Ulusoy et al., "~3-nm ZnO nanoislands deposition and application in charge trapping memory grown by single ALD step," *Scientific Reports*, vol. 6, no. 1, article 38712, 2016.

[64] K. S. Ahmad and S. B. Jaffri, "Phytosynthetic Ag doped ZnO nanoparticles: semiconducting green remediators," *Open Chemistry*, vol. 16, no. 1, pp. 556–570, 2018.

[65] S. S. Shinde, C. H. Bhosale, and K. Y. Rajpure, "Oxidative degradation of acid orange 7 using Ag-doped zinc oxide thin films," *Journal of Photochemistry and Photobiology B: Biology*, vol. 117, pp. 262–268, 2012.

[66] S. Jayswal and R. S. Moirangthem, "Construction of a solar spectrum active SnS/ZnO p–n heterojunction as a highly efficient photocatalyst: the effect of the sensitization process on its performance," *New Journal of Chemistry*, vol. 42, no. 16, pp. 13689–13701, 2018.

[67] S. J. Park, G. S. Das, F. Schütt et al., "Visible-light photocatalysis by carbon-nano-onion-functionalized ZnO tetrapods: degradation of 2,4-dinitrophenol and a plant-model-based ecological assessment," *NPG Asia Materials*, vol. 11, no. 1, article 107, p. 8, 2019.

[68] S. Kuriakose, B. Satpati, and S. Mohapatra, "Highly efficient photocatalytic degradation of organic dyes by Cu doped ZnO nanostructures," *Physical Chemistry Chemical Physics*, vol. 17, no. 38, pp. 25172–25181, 2015.

[69] C. Diaz-Uribe, W. Vallejo, and W. Ramos, "Methylene blue photocatalytic mineralization under visible irradiation on TiO_2 thin films doped with chromium," *Applied Surface Science*, vol. 319, pp. 121–127, 2014.

[70] A. V. Emeline, V. N. Kuznetsov, V. K. Ryabchuk, and N. Serpone, "Chapter 1-Heterogeneous photocatalysis: basic approaches and terminology," in *New and Future Developments in Catalysis*, pp. 1–47, Elsevier, 2013.

[71] K. Ishibashi, A. Fujishima, T. Watanabe, and K. Hashimoto, "Quantum yields of active oxidative species formed on TiO_2 photocatalyst," *Journal of Photochemistry and Photobiology A: Chemistry*, vol. 134, no. 1-2, pp. 139–142, 2000.

[72] O. Legrini, E. Oliveros, and A. M. Braun, "Photochemical processes for water treatment," *Chemical Reviews*, vol. 93, no. 2, pp. 671–698, 1993.